Catalysis Letters (2018) 148:214–219
https://doi.org/10.1007/s10562-017-2251-x

$Co_3(PO_4)_2$ Nanoparticles Embedded in Nitrogen-Doped Carbon as an Advanced Electrocatalyst for OER in Alkaline Solution

Pingjing Feng[1] · Xian Cheng[1] · Jintang Li[1] · Xuetao Luo[1]

Received: 16 September 2017 / Accepted: 7 November 2017 / Published online: 24 November 2017

Abstract

The advanced oxygen evolution catalysts in alkaline solution play a growing role in alternative energy devices due to the need for clean and sustainable energy. In this paper, we report the cobalt phosphate nanoparticles embedded in N-doped carbon ($Co_3(PO_4)_2$@N-C) using *N,N′*-piperazinebis (methylene-phosphonic acid) as both phosphate and carbon sources by two-step, hydrothermal method. The prepared $Co_3(PO_4)_2$@N-C annealed at 600 °C exhibits advanced OER performance, with a current density of 10 mA cm^{-2} at a lower overpotential of 290 mV, a Tafel slope of 82 mV dec^{-1} and superior durability in 1.0 M KOH solution. This kind of material with MOF as precursor has wide application prospect in electro-chemistry field, especially for OER.

Graphical Abstract

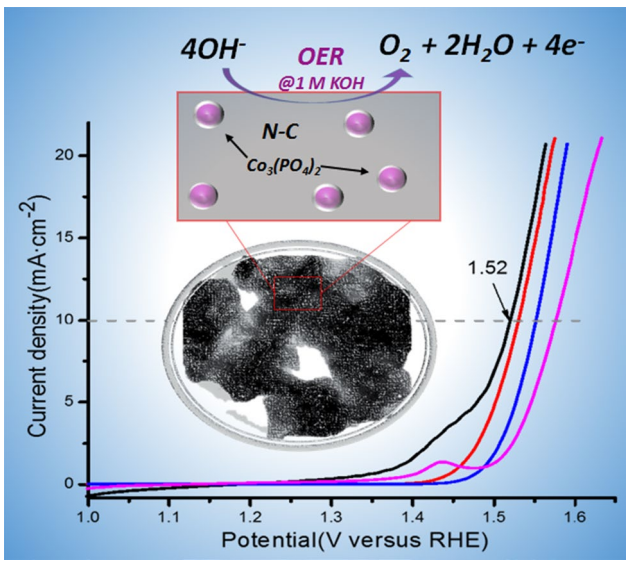

Keywords Cobalt phosphate · Nanoparticles · Nitrogen-doped carbon · Oxygen evolution reaction

1 Introduction

The oxygen evolution reaction (OER) and the hydrogen evolution reaction (HER) are important for the water splitting [1]. The HER is a relatively simple reaction that is easily prone to many materials in a low potential [2]. Nevertheless, the OER is a more complicated reaction

Electronic supplementary material The online version of this article (https://doi.org/10.1007/s10562-017-2251-x) contains supplementary material, which is available to authorized users.

✉ Jintang Li
leejt@xmu.edu.cn

[1] Fujian Key Laboratory of Advanced Materials, College of Materials, Xiamen University, Xiamen 361005, Fujian, China

with higher overpotential, because there are four successive electron transfer procedures and low kinetics [3–5]. Generally, in the OER, the thermodynamic potential value is 1.23 V at about 25 °C (vs RHE) [6]. However, for the presence of the extra potential (also called overpotential), we must adopt to a higher potential to promote the electrocatalytic OER reaction. Thus, significant efforts have been made to explore highly efficient electrocatalysts for the OER.

Metal–organic frameworks (MOFs), as the superior electrocatalysts in aqueous alkaline solutions, have received notable attention in recent years due to the structural and chemical multiformity [7–9]. MOFs have become popular as pyrolytic precursors for synthesis of porous electrocatalysts [10–13]. MOFs are easily prepared with metal@N-C components that are well scattered within the frameworks and can be transformed into active metal@N-C structures for OER/ORR by an annealing procedure [14–17]. For instance, Zhang et al. reported a porous Co_3O_4/C nanowire prepared through thermally annealing a Co-based MOF, which can be used as catalysts for OER [18]. Lin et al. synthesized Co_9S_8@CoS@CoO@C nanoparticles using MOF as the precursor, which possessed excellent catalytic activity for the OER [19].

To date, transition metal phosphides have aroused widespread concern, owing to their plentiful reserves, environmental-friendly property [20–23]. In recent years, in order to enhance the electrocatalytic activity of transition metal phosphides electrocatalysts, various cobalt-containing phosphides have been prepared. Meanwhile, a number of cobalt phosphides or cobalt phosphates have been investigated as the OER electrocatalysts [21, 24, 25]. For example, Li et al. reported the Co-Pi electrocatalyst modified TiO_2 nanowire with co-catalytic effect, which had excellent catalytic properties [26].

Herein, we prepared the cobalt phosphate nanoparticles embedded in N-doped carbon ($Co_3(PO_4)_2$@N-C) through hydrothermal method. During the synthesis process, $Co(NO_3)_2{\cdot}6H_2O$ reacted with *N,N″*-piperazinebis(methylenephosphonic acid) (PMP) in water by hydrothermal method, then the obtained precipitate was annealed at 600, 700, 800, 900 °C for 3 h in air to get $Co_3(PO_4)_2$@N-C catalysts. The PMP not only acted as the phosphate source, but also was thermally decomposed into N doped carbon (N-C) coating on cobalt phosphate nanoparticles during the pyrolysis process, which enhanced the electrocatalytic performance. The prepared $Co_3(PO_4)_2$@N-C annealed at 600 °C exhibits a current density of 10 mA cm^{-2} at a lower overpotential of 290 mV in 1.0 M KOH solution. Besides, the catalysts have good catalytic stability over continuous 1000 cycles with negligible drops of the current density, and little decay (5.7%) in OER activity up to 8 h of continuous operation at 1.52 V versus RHE.

2 Experimental

2.1 Chemicals

All reagents were used without further purification. Cobalt nitrate hexahydrate ($Co(NO_3)_2{\cdot}6H_2O$, Shanghai Titanchem Co. Ltd., ≥ 99.8%), PMP was prepared by the method reported by Alhendawi et al. [27]. Potassium hydroxide (KOH, Shanghai Titanchem Co. Ltd., ≥ 85.0%). Distilled water was utilized in all experimental procedures.

2.2 Synthesis of Cobalt Phosphate Catalysts

Generally, 2.46 mmol (0.716 g) of $Co(NO_3)_2{\cdot}6H_2O$ was dissolved in 20 mL of distilled water under magnetic stirring, then 1.23 mmol (0.337 g) of PMP was added. 1.0 M KOH solution was added dropwise to the mixture to adjust a final reaction pH of 7. The mixture was stirred for another 10 min, and transferred to Teflon-lined stainless steel autoclave and maintained at 200 °C for 72 h. After being cooled to room temperature, the purple powder was filtered under vacuum and washed thoroughly with distilled water. Dried at 60 °C overnight. As-prepared purple powder was named Co-PMP. To obtain the final product, the Co-PMP powder was then annealed at 600, 700, 800, 900 °C in air at a heating rate of 5 °C min^{-1}. After kept at different temperature for 3 h, the powder was cooled down to room temperature at a cooling rate of 5 °C min^{-1}. Finally, purple $Co_3(PO_4)_2$@N-C powder at different temperature was obtained.

2.3 Characterization

X-ray diffraction (XRD) patterns were performed on a Bruker-Axs D8 Advance X-ray diffractometer in a wide angle range($2\theta = 5–35°$) with Cu K_α radiation, operating at 40 kV and 40 mA. The morphology of the samples was operated on SU70 field-emission scanning electron microscopy (FE-SEM) instrument at 10 kV, and elemental mappings were obtained at 20 kV. Samples for SEM were gold sputtered before the analyses. The high-resolution transmission electron microscopy (HRTEM) characterization was carried out on a Tecnai F30 microscope at an accelerating voltage of 300 kV. N_2 adsorption–desorption isotherms were employed on a Quantachrome NOVA 2000e sorption analyzer (Fig. S2). The X-ray photoelectron spectroscopy (XPS) data was acquired on an ESCALAB 250Xi X-ray photoelectron spectrometer (Thermo Scientific) using Al K_α radiation. TG were performed in Netzsch STA449 F3 Jupiter (Fig. S3).

2.4 Evaluation of the Electrocatalytic Activity Toward OER

Cyclic voltammetry (CV) and linear sweep voltammetry (LSV) measurements were carried out on an Autolab electrochemical workstation (NOVA 2.1). The catalytic activity for OER was evaluated at room temperature in a conventional three-electrode system with electrochemical workstation in 1.0 M KOH solution. The electrode of glassy carbon (5 mm diameter, 0.196 cm^2) was used as the working electrode. The Pt foil and an Ag/AgCl-saturated electrode were used as the counter electrode and reference electrode. In order to prepare the working electrode, 5 mg of catalysts were dispersed in a mixture of 950 µL ethanol and 50 µL 5 wt% Nafion solution with sonication for 60 min. After this process, the catalysts (20 µL) were dropped onto a glassy carbon electrode and then fully dried at room temperature for 12 h before measurements (loading ~0.510 mg cm^{-2}). Linear sweep voltammetry was carried out at a scan rate of 10 mV S^{-1} for the polarization curves from 1.0 to 1.7 V. All the measured potentials were referred to RHE with the following equation: $E\,(RHE) = E_{Ag/AgCl} + 0.197 + 0.059pH$.

3 Results and Discussion

To obtain the final products, the Co-PMP powder was then annealed at different temperature. Because the electrochemical reaction of the amorphous products calcined at below 600 °C was very complex, in which both anode and cathode reaction were included, we chose samples of other temperatures for the OER test. Figure 1 presented the PXRD pattern of $Co_3(PO_4)_2$@N-C powder annealed at different temperature (600, 700, 800 and 900 °C). The diffraction pattern exhibits peak at 20.52°, 21.91°, 25.65°, 27.68° and 36.78°, corresponding to (011), (101), (210), (021) and (031) planes of $Co_3(PO_4)_2$ (JCPDS No. 77-0225), respectively. No peaks from carbon and nitrogen are observed, because of the low concentration; In addition, peaks appearing in 29.62°, 30.14° can be indexed to $Co_2P_2O_7$ (JCPDS No. 34-1378), indicating that a small amount of $Co_2P_2O_7$ was doped in the $Co_3(PO_4)_2$@N-C. This phenomenon increases the number of active coordinated sites and can be beneficial to electrocatalytic application for OER. Obviously, with the increase of pyrolysis temperature, the crystallinity was getting better. With the increase of the thermal treatment temperature, the internal defects of the material gradually decreased, and the carbon element gradually disappeared (Table S2 see Supporting Information).

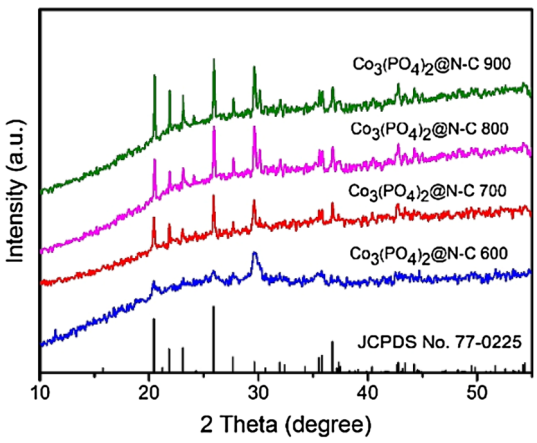

Fig. 1 PXRD pattern of $Co_3(PO_4)_2$@N-C annealed at 600, 700, 800 and 900 °C

The electrocatalytic activity of $Co_3(PO_4)_2$@N-C catalysts at different temperature (600, 700, 800 and 900 °C) for OER was also evaluated (Fig. 2). The Tafel slope can be fitted to an equation: $\eta = b\log(J) + a$, where η presents the overpotential and current density is indicated by *J, b* is the Tafel slope. As shown in Fig. 2a, b, the overpotential at a current density of 10 mA cm^{-2} were 290, 300, 320, 340 mV, respectively; Besides, the corresponding Tafel slope were 82, 97, 126, 101 mV dec^{-1}, respectively. The overpotential at a current density of 10 mA cm^{-2} and Tafel slope are important metrics, a good OER electrocatalyst should possess a low overpotential and Tafel slope, therefore, the $Co_3(PO_4)_2$@N-C products annealed at 600 °C were much superior to others. To summarize, according to the results of PXRD (Fig. 1) and N_2 adsorption–desorption isotherms (Fig. S2 see Supporting Information), we surmised that there are three reasons for the good OER performance of the $Co_3(PO_4)_2$@N-C catalysts annealed at 600 °C. Firstly, the $Co_3(PO_4)_2$@N-C catalysts annealed at 600 °C belong to poor crystallinity material, which also were doped with $Co_2P_2O_7$. Compared with the better crystalline materials, there will be more active sites because of the presence of the small clusters caused by the internal defects [28, 29]; Then, the $Co_3(PO_4)_2$@N-C catalysts annealed at 600 °C possess the larger specific surface areas, which could increase the density of the surface reactive sites and the contact areas [30]. Finally, the N-doped carbon layers act as a bridge linking nanoparticles, which can enhance the electrochemical performance [31]. The stability of $Co_3(PO_4)_2$@N-C catalysts for OER was measured by the i–t tests at a constant potential of 1.52 V versus RHE, it can be clearly seen that $Co_3(PO_4)_2$@N-C catalysts annealed at 600 °C exhibit superior durability, with little decay (5.7%) in OER activity up to 8 h of continuous operation (Fig. 2c). Further stability test showed that the $Co_3(PO_4)_2$@N-C catalysts annealed at 600 °C almost consistent with the OER polarization curves as initial catalyst after 1000 cycles, only with negligible increases of the overpotential (Fig. 2d).

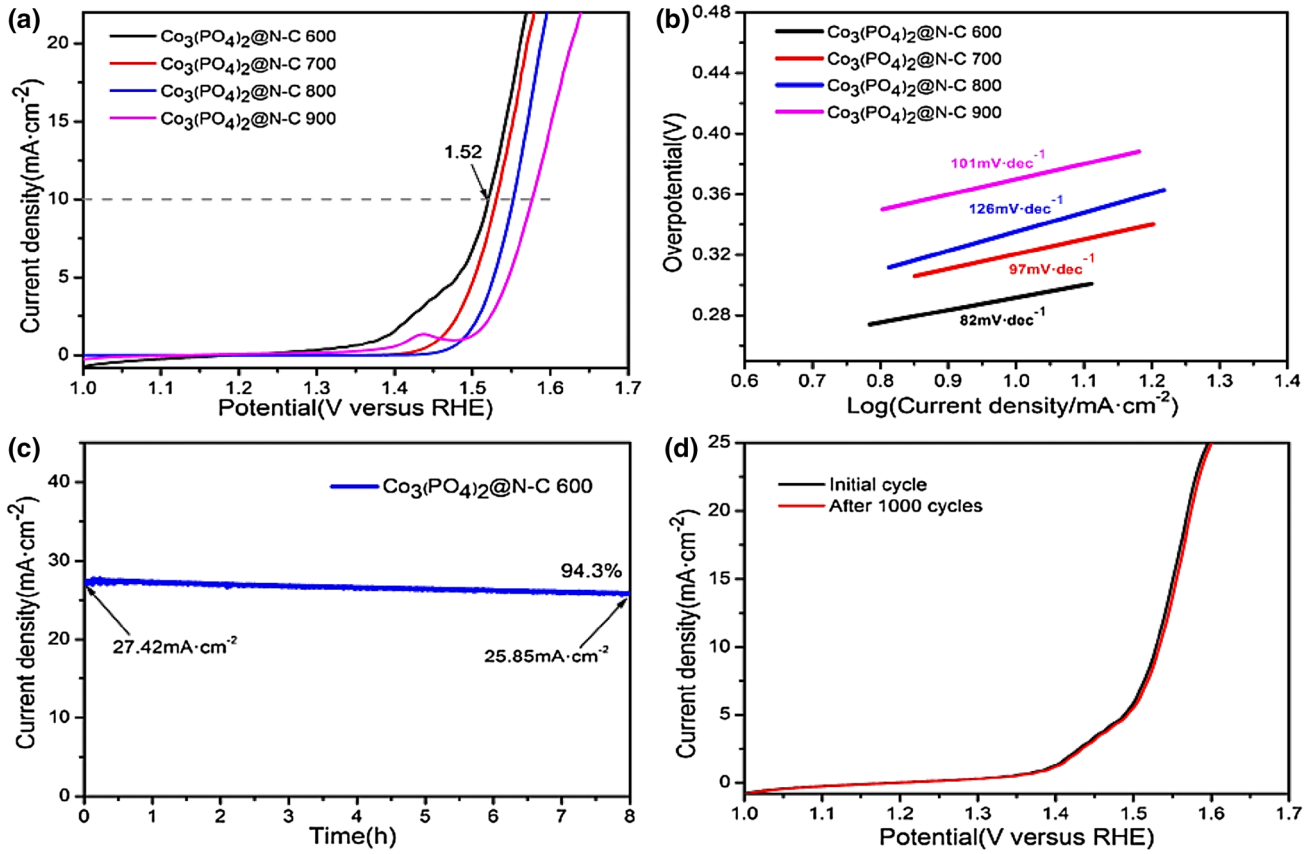

Fig. 2 **a** OER polarization curves of $Co_3(PO_4)_2$@N-C annealed at 600, 700, 800 and 900 °C, sweep rate: 10 mV S^{-1} in 1 M KOH. **b** Corresponding Tafel slope plots. **c** The i–t curve of $Co_3(PO_4)_2$@N-C annealed at 600 °C at 1.52 V versus RHE. **d** OER polarization curves of $Co_3(PO_4)_2$@N-C annealed at 600 °C before and after 1000 cycles

To get an in-depth understanding of the morphology and element composition of the top OER performance catalysts, which are $Co_3(PO_4)_2$@N-C nanoparticles annealed at 600 °C, scanning electron microscopy (SEM) and transmission electron microscopy (TEM) were obtained (in Fig. 3). As shown in Fig. 3a–c, it can be observed that the sample contains a great number of nanoparticles with diameter about 200 nm. In addition, SEM images and the corresponding elemental mappings of the $Co_3(PO_4)_2$@N-C catalysts annealed at 600 °C are shown in Fig. 3d–i, which present $Co_3(PO_4)_2$@N-C composites were mainly comprised of cobalt, phosphorus and oxygen with trace amounts of carbon and nitrogen elements, inferring that pyrolysis process from Co-PMP can obtain nitrogen-doped carbon scaffold encapsulated in situ with $Co_3(PO_4)_2$ nanoparticles. The N-doped carbon layers act as a network connection structure, which may enhance the electrochemical kinetics and further improve the OER performance.

The XPS was used to characterize the elements state of the $Co_3(PO_4)_2$@N-C catalysts annealed at 600 °C (Fig. S4 see Supporting Information). The full XPS spectra provided evidence for presence of Co, P, O, and N as well as C (Fig. S4a). As shown in Fig. S4b, for the Co 2p XPS spectrum, two major peaks of $2p_{3/2}$ and $2p_{1/2}$ (resulting from the spin–orbit splitting), located at 781.7 and 797.8 eV, respectively, which can be assigned to Co^{2+} [32, 33]. The P 2p spectrum (Fig. S4c) clearly demonstrates the existence of phosphorus atoms in two chemical environment. The P 2p XPS displays two peaks, the $2p_{3/2}$ and $2p_{1/2}$ peaks were observed at 133.4 and 134.4 eV binding energies [34, 35]. The O 1s spectrum can be discovered by two sub-peaks (Fig. S4d), centred at 531.5 and 533 eV, which are characteristics of O^{2-} ions in oxygen-deficient regions within the matrix of $Co_3(PO_4)_2$ nanoparticles. Two peaks at 400.1 and 403.7 eV in the N 1s spectrum can be attributed to the presence of pyrrolic-type nitrogen atoms and the oxidized nitrogen, respectively (Fig. S4e) [36]. There are three resolved peaks in the C 1s spectrum. The first peak present at 284.7 eV, which is characteristic of C–C peak; The other two peaks centered at 285.8 and 287.8 eV were assigned to carbon binding with surface nitrogen and oxygen groups (C–N, C=O) respectively [37–40].

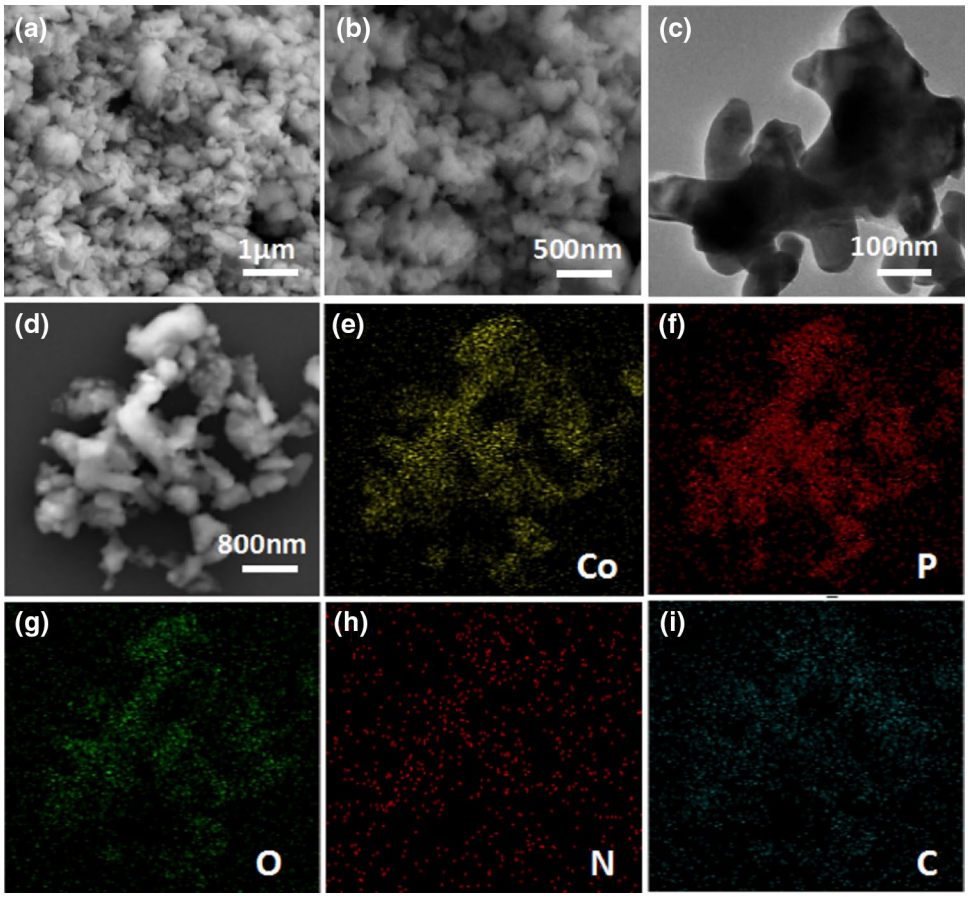

Fig. 3 **a, b** SEM images of $Co_3(PO_4)_2$@N-C catalysts annealed at 600 °C at different magnification. **c** TEM image. **d–i** SEM image and the corresponding elemental mappings

4 Conclusion

In summary, we prepared cobalt phosphate nanoparticles embedded in N-doped carbon ($Co_3(PO_4)_2$@N-C annealed at 600 °C), which are prepared via a simple hydrothermal process using PMP as both the phosphate source and carbon source. The obtained materials display superior electrocatalytic activity for OER. Firstly, the N-doped carbon layers act as a bridge linking nanoparticles, which can enhance the electrochemical performance. Then, small amounts of doping of $Co_2P_2O_7$, the poor crystallinity and larger specific surface areas contribute to more active sites and contact areas, improving the catalytic activity and stability efficiently.

References

1. Zou XX et al (2013) Efficient oxygen evolution reaction catalyzed by low-density Ni-doped Co_3O_4 nanomaterials derived from metal-embedded graphitic C_3N_4. Chem Commun 49(68):7522–7524
2. Landon J et al (2012) Spectroscopic characterization of mixed Fe–Ni oxide electrocatalysts for the oxygen evolution reaction in alkaline electrolytes. ACS Catal 2(8):1793–1801
3. Najafpour MM et al (2012) Nano-sized manganese oxide-bovine serum albumin was synthesized and characterized. It is promising and biomimetic catalyst for water oxidation. RSC Adv 2(30):11253–11257
4. Chen S et al (2013) Three-dimensional N-doped graphene hydrogel/NiCo double hydroxide electrocatalysts for highly efficient oxygen evolution. Angew Chem Int Ed 52(51):13567–13570
5. Kanan MW, Nocera DG (2008) In situ formation of an oxygen-evolving catalyst in neutral water containing phosphate and Co^{2+}. Science 321(5892):1072–1075
6. Han L, Dong SJ, Wang EK (2016) Transition-metal (Co, Ni, and Fe)-based electrocatalysts for the water oxidation reaction. Adv Mater 28(42):9266–9291
7. Chaikittisilp W et al (2014) Synthesis of nanoporous carbon–cobalt–oxide hybrid electrocatalysts by thermal conversion of metal–organic frameworks. Chemistry 20(15):4217–4221
8. Gascon J et al (2014) Metal organic framework catalysis: Quo vadis? ACS Catal 4(2):361–378
9. Xia W et al (2015) Metal-organic frameworks and their derived nanostructures for electrochemical energy storage and conversion. Energy Environ Sci 8(7):1837–1866
10. Xu X et al (2012) Spindle-like mesoporous alpha-Fe_2O_3 anode material prepared from MOF template for high-rate lithium batteries. Nano Lett 12(9):4988–4991
11. Zhao SL et al (2014) Carbonized nanoscale metal–organic frameworks as high performance electrocatalyst for oxygen reduction reaction. ACS Nano 8(12):12660–12668
12. Wang H et al (2014) Preparation, characterization and bifunctional catalytic properties of MOF(Fe/Co) catalyst for oxygen reduction/

evolution reactions in alkaline electrolyte. Int J Hydrog Energy 39(28):16179–16186
13. Shang NZ et al (2016) Ag/Pd nanoparticles supported on amine-functionalized metal–organic framework for catalytic hydrolysis of ammonia borane. Int J Hydrog Energy 41(2):944–950
14. Dou S et al (2016) Etched and doped Co_9S_8/graphene hybrid for oxygen electrocatalysis. Energy Environ Sci 9(4):1320–1326
15. Yu HY et al (2016) Cu, N-codoped hierarchical porous carbons as electrocatalysts for oxygen reduction reaction. ACS Appl Mater Interfaces 8(33):21431–21439
16. Ma TY et al (2016) Interacting carbon nitride and titanium carbide nanosheets for high-performance oxygen evolution. Angew Chem Int Ed 55(3):1138–1142
17. Liu YY et al (2016) Transition metals (Fe, Co, and Ni) encapsulated in nitrogen-doped carbon nanotubes as bi-functional catalysts for oxygen electrode reactions. J Mater Chem A 4(5):1694–1701
18. Ma TY et al (2014) Metal–organic framework derived hybrid Co_3O_4-carbon porous nanowire arrays as reversible oxygen evolution electrodes. J Am Chem Soc 136(39):13925–13931
19. Long JY, Gong Y, Lin JH (2017) Metal–organic framework-derived Co_9S_8@CoS@CoO@C nanoparticles as efficient electro- and photo-catalysts for the oxygen evolution reaction. J Mater Chem A 5(21):10495–10509
20. Bendi R et al (2016) Metal organic framework-derived metal phosphates as electrode materials for supercapacitors. Adv Energy Mater 6(3)
21. Li XY et al (2016) ZIF-67-derived Co-NC@CoP-NC nanopolyhedra as an efficient bifunctional oxygen electrocatalyst. J Mater Chem A 4(41):15836–15840
22. Liu YR et al (2016) Novel CoP hollow prisms as bifunctional electrocatalysts for hydrogen evolution reaction in acid media and overall water-splitting in basic media. Electrochim Acta 220:98–106
23. Pu ZH et al (2017) General strategy for the synthesis of transition-metal phosphide/N-doped carbon frameworks for hydrogen and oxygen evolution. ACS Appl Mater Interfaces 9(19):16187–16193
24. Chang JF et al (2015) Surface oxidized cobalt-phosphide nanorods as an advanced oxygen evolution catalyst in alkaline solution. ACS Catal 5(11):6874–6878
25. Surendranath Y, Kanan MW, Nocera DG (2010) Mechanistic studies of the oxygen evolution reaction by a cobalt-phosphate catalyst at neutral pH. J Am Chem Soc 132(46):16501–16509
26. Ai GJ et al (2015) Cobalt phosphate modified TiO_2 nanowire arrays as co-catalysts for solar water splitting. Nanoscale 7(15):6722–6728
27. Alhendawi H et al (2013) A new layered zirconium biphosphonate framework covalently pillared with *N,N′*-piperazinebis(methylene) moiety: synthesis and characterization. J Porous Mater 20(5):1189–1194
28. Zhou W et al (2011) Amorphous iron oxide decorated 3D heterostructured electrode for highly efficient oxygen reduction. Chem Mater 23(18):4193–4198
29. Bergmann A et al (2015) Reversible amorphization and the catalytically active state of crystalline Co_3O_4 during oxygen evolution. Nat Commun 6:8625
30. Zhao J et al (2014) Self-template construction of hollow Co_3O_4 microspheres from porous ultrathin nanosheets and efficient noble metal-free water oxidation catalysts. Nanoscale 6(13):7255–7262
31. Chen ZY et al (2017) Ag-enhanced catalytic performance of ordered mesoporous Fe–N-graphitic carbons for oxygen electroreduction. Catal Lett 147(11):2745–2754
32. Yang J et al (2010) Synthesis and characterization of cobalt hydroxide, cobalt oxyhydroxide, and cobalt oxide nanodiscs. J Phys Chem C 114(1):111–119
33. Xing M et al (2014) Cobalt vanadate as highly active, stable, noble metal-free oxygen evolution electrocatalyst. J Mater Chem A 2(43):18435–18443
34. Hu GR et al (2008) Comparison of $AlPO_4$- and $Co_3(PO_4)(2)$-coated $LiNi_{0.8}Co_{0.2}O_2$ cathode materials for Li-ion battery. Electrochim Acta 53(5):2567–2573
35. Yuan CZ et al (2016) Cobalt phosphate nanoparticles decorated with nitrogen-doped carbon layers as highly active and stable electrocatalysts for the oxygen evolution reaction. J Mater Chem A 4(21):8155–8160
36. Zhang CZ et al (2013) Synthesis of amino-functionalized graphene as metal-free catalyst and exploration of the roles of various nitrogen states in oxygen reduction reaction. Nano Energy 2(1):88–97
37. Nagaiah TC et al (2012) Mesoporous nitrogen-rich carbon materials as catalysts for the oxygen reduction reaction in alkaline solution. ChemSusChem 5(4):637–641
38. Shruthi TK et al (2014) Functionalization of graphene with nitrogen using ethylenediaminetetraacetic acid and their electrochemical energy storage properties. RSC Adv 4(46):24248–24255
39. Li XZ et al (2015) MOF derived Co_3O_4 nanoparticles embedded in N-doped mesoporous carbon layer/MWCNT hybrids: extraordinary bi-functional electrocatalysts for OER and ORR. J Mater Chem A 3(33):17392–17402
40. Zhou WJ et al (2015) N-doped carbon-wrapped cobalt nanoparticles on N-doped graphene nanosheets for high-efficiency hydrogen production. Chem Mater 27(6):2026–2032